NUMERICAL AND EXPERIMENTAL EVALUATION OF CALM WATER RESISTANCE AND INTERFERENCE EFFECTS FOR HYDROFOIL-ASSISTED SWATH

Ezzul Hanis Othman[a], Arifah Ali[b]*, Adi Maimun Abd. Malik[c], M. Hazmil Shahidy Abdol Azis[c], Chee-Loon Siow[b], Hooi-Siang Kang[b], Adibah Fatihah Mohd Yusof[a]

[a]Faculty of Mechanical Engineering, Universiti Teknologi Malaysia,81310 UTM Johor Bahru, Johor, Malaysia
[b]Marine Technology Center, Universiti Teknologi Malaysia, 81310 UTM Johor Bahru, Johor, Malaysia.
[c]Department of Aeronautics, Automotive and Ocean Engineering, Faculty of Mechanical Engineering, 81310 UTM Johor Bahru, Johor, Malaysia.

*Corresponding email: arifahali@utm.my

Article history
Received
11th November 2025
Revised
9th April 2026
Accepted
9th April 2026
Published
3rd June 2026

ABSTRACT

The purpose of this study is to evaluate the interference factor of a conventional Small Waterplane Area Twin Hull (SWATH) vessel with and without the hydrofoils in calm water. While integrating hydrofoils into SWATH designs can reduce wetted surface area and improve hydrodynamic efficiency, it also introduces complex hydrodynamic phenomena and interference effects at the free surface. Conventional methods for calculating interference factors have proven inadequate for hydrofoil-assisted SWATH designs, necessitating a more robust analytical approach. To address this, a modified equation using the resistance coefficient was developed, specifically considering the running wetted surface area of each individual component of the vessel. The methodology involved the construction of a SWATH model featuring passive NACA 0015 hydrofoils in a tandem configuration at the forward and aft ends. Resistance tests were conducted in a towing tank across a range of Froude numbers (Fr) from 0.28 to 0.48, complemented by numerical simulations performed using OpenFOAM to analyze the flow field and wave patterns. A central aspect of this study is the implementation of a new formula for the interference factor that accounts for the dynamic change in the running wetted surface area of the demi-hulls and hydrofoils to improve calculation accuracy. Results indicated that the addition of hydrofoils increased the total resistance coefficient by average 21%. Despite this increase, the hydrofoils significantly improved pitch and heave motions by providing essential dynamic lift. Notably, numerical results identified a zone of beneficial (destructive) wave interference at Fr = 0.38, where overall wave making energy was effectively reduced. The study concludes that hydrofoil-assisted SWATH exhibits a higher interference factor than the bare hull. Furthermore, the findings demonstrate that conventional equations are unsuitable for hydrofoil-integrated multihulls, validating the necessity of the modified resistance coefficient equation introduced in this work.

Keywords: *Calm water resistance, hydrofoils, interference effect, multihull resistance, SWATH, CFD OpenFOAM*

1.0 INTRODUCTION

The advancement of naval architecture and marine engineering has always relied on exploring efficient marine vessels. The Small Waterplane Area Twin Hull (SWATH) is notable among many vessels designs for its unique structural and hydrodynamic features. SWATH is known as a craft with excellent seakeeping behaviour [1] consisting of a slender strut that acts as wave-piercing at the free surface. It also has a smaller design waterplane area-to-hull volumetric displacement ratio than a monohull or traditional catamaran [2].

Some appendages are required to maintain the relatively small waterplane area of the SWATH for medium and high-speed application. Extensive research has been carried out to investigate the appendage effect for SWATH-type vessel. Wang *et. al* [3] designed two double-strut USV-SWATH with and without hydrofoils. The hydrofoil shape defined by the authors resembles the fin stabilizer geometry used by Begovic *et. al* [1], Wang *et. al* [4], Sun *et. al* [5], Ali *et. al* [6], and Rahimuddin [7], suggesting a comparable hydrodynamic behavior between the present and previous studies.

Hydrofoils are commonly used to improve vessels' performance, particularly monohulls and catamarans [8-11], to enhance hydrodynamic efficiency by reducing their wetted surface area [12]. Their efficiency rises with the square of the speed before cavitation or separation occurs on the hydrofoil surface. According to Migeotte and Hoppe [11] and Putranto and Sulisetyono [13], hydrofoils are useful because they provide dynamic lift, which is helpful when a vessel travels at medium and high speeds. Thus, it extends a vessel application on the conventional hull. This is because, at low speeds, hydrofoils do not generate much lift and, instead, act as passive viscous dampers [14]. Their ability to produce large restoring forces and moments makes hydrofoil more like other heave and pitch reduction devices [15].

Karim *et. al* [16] and Prasad *et. al* [17] numerically investigated the free surface generated by the flow around NACA 0015 and NACA 0012 hydrofoils. Under the same numerical scheme, Uddin and Karim [18] examine the influence of the free surface on NACA 4412 hydrofoil at varied submergence ratios (h/c) within intervals of $1 \leq h/c \leq 5$. They found that the lift coefficient (C_L) increased, and the total resistance coefficient (C_T), decreased gradually with an increase in h/c. In other research, Ni *et. al* [12] evaluated the performance of NACA 634-021 hydrofoil operating closer to a free surface with h/c values of 0.5c, 1.0c, and 1.5c. They found that the motion-induced surface wave may enhance the hydrofoil's performance at certain h/c values, especially 0.5c, at which there is some delay in the stall. This enhancement improved the hydrofoil's performance within the interval of $17^o \leq AoA \leq 30^o$.

While the benefits of hydrofoils in marine applications are well-documented, their introduction to the SWATH vessel may introduce complex hydrodynamic phenomena including interference effect at the free surface. These interference effects, if not thoroughly understood and managed, can disprove the potential advantages of hydrofoil integration. Thus, this paper aims to evaluate the interference factor of a conventional SWATH with and without hydrofoils in calm water. Specifically, it examines the use of hydrofoils (NACA 0015) in tandem configuration on a SWATH model, with the goal of combining the efficiency benefits of hydrofoils while minimizing their drawbacks related to resistance.

2.0 METHODOLOGY

2.1 Model Description

The SWATH model was constructed featuring passive NACA 0015 hydrofoils fastened to both the forward and aft ends of the structure. Table 1 shows the main details and properties of the model. Figure 1 shows the model installed on the towing carriage during model test

with 23.6°C tank water temperature used for determination of fluid properties. The data from model testing is used for validation of the OpenFOAM simulation result.

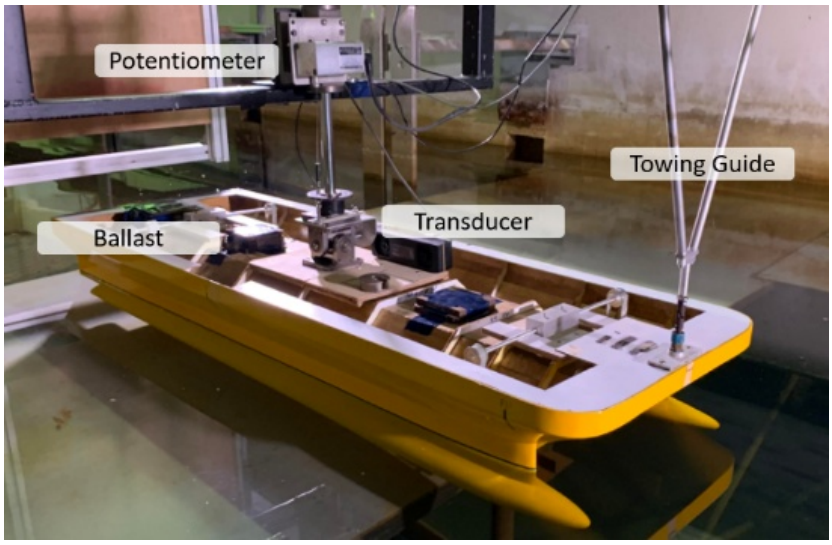

Figure 1: Model test setup.

The size of hydrofoils is the same as the dimensions shown in Table 2. These locations were based on the positions proposed by Ochi [19]. They were placed within 10% of the ship model's length measured from the end where the NACA 0015 hydrofoils were located, as shown in Figure 2. The authors reported that a greater distance to the centre of the ship's rotation yields more effective results. This placement methodology aligns with models developed by Rahimuddin [7] and Ali [20].

Table 1: Details of the SWATH model.

Parameters	Unit	Values
Displacement, Δ	kg	15.02
Length at the waterline, L_{WL}	m	1.194
Overall length, L_{OA}	m	1.290
Beam of demi hull at waterline, B_{Demi}	m	0.039
Draft at the midship, T	m	0.110
Longitudinal centre of gravity, LCG	m	0.627
Vertical centre of gravity, VCG	m	0.173
Pitch radius of gyration, k_{yy}	m	0.334

Table 2: Details of the hydrofoils.

Parameters	Unit	Forward	Aft
Chord, c	m	0.100	
Span, b	m	0.256	
Maximum Thickness	m	0.014	
Hydrofoil aspect ratio, AR		2.560	

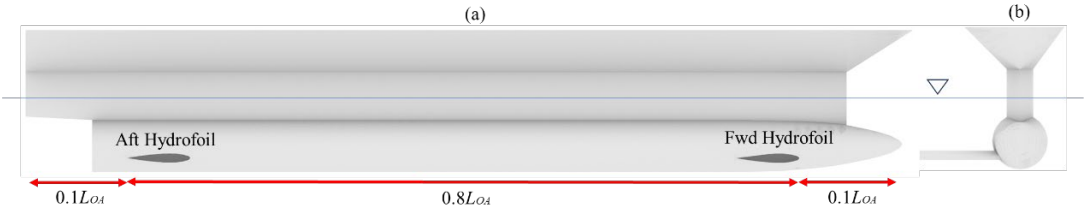

Figure 2: SWATH model and location of the hydrofoils, (a) Profile view; (b) Front view

2.2 *Resistance Coefficient of the Multihull*

A series of resistance tests were conducted in calm water to obtain experimental data for validating the CFD results. The Froude numbers (F_r) used in this study were within the interval of $0.28 \leq F_r \leq 0.48$, corresponding to the model forward velocity of 1.0 m/s $\leq U_M \leq$ 1.71 m/s (see Table 3). According to ITTC 1957, the dimensionless resistance coefficient was obtained from Equation 1. This formula was recommended by ITTC'57 under code 7.5-02-01-03, and the procedure was followed closely. The running wetted surface area, S_M, is used because the wetted area changes significantly with the speed response from the generated lift [21].

Table 3: Ship speed for model and full scale correspond to Froude number.

Froude Number	Model Scale (m/s)	Full Scale (knots)
0.28	1.00	11
0.33	1.17	13
0.38	1.35	15
0.48	1.71	18

$$C_{TM} = \frac{R_{TM}}{\frac{1}{2}\rho S_M U^2} \tag{1}$$

In this study, the appendage resistance coefficient, C_{AppM} was contributed by NACA 0015 hydrofoils, which were broken into two components – forward (C_{H1}) and aft (C_{H2}), as shown in Equation 2. These values were calculated by performing the test with and without appendages. However, the potential for structural damage or cracks during the attachment and detachment of hydrofoils limited their consideration to numerical simulations. Meanwhile, S_0 is a nominal wetted surface value, for instance, at zero speed (hull at rest).

$$C_{TM} = C_{FM}\frac{S_M}{S_{S0}} + C_R + C_{H1} + C_{H2} \tag{2}$$

2.3 Numerical Setup

The simulations were performed for Froude numbers of $0.28 \leq Fr \leq 0.48$ at $h/c = 0.9$. This stage is crucial as minimizing relative errors enhances the accuracy of the simulation results. The flow field is governed by the incompressible Navier–Stokes equations, which express conservation of mass and momentum for Newtonian fluids. It was further used to investigate the interference factor and effects of the hydrofoils on the model. The interference factor was calculated by comparing the model with interference to the model without interference. The value of hydrofoils-assisted SWATH without interference was

obtained by the sum of the total between the model parts calculated separately between the demi-hulls, forward, and aft hydrofoils.

2.3.1 Computational Domain and Grid

The computational domain for the multiphase cases was divided into two regions (air and water) separated by a free surface, as shown in Figure 3. The fluid properties for simulation (OpenFOAM), was determined according to the experimental conditions. The water temperature was measured using a thermometer. Based on the ITTC 1957 procedure (Code 7.5-02-01-03), the freshwater properties at 23.6 °C were calculated using the data provided in Table 4. Through interpolation, the density (ρ) and dynamic viscosity (μ) were determined to be 997.396 kgm^{-3} and 9.236×10^{-4} Pa.s, respectively. Then, the corresponding kinematic viscosity (v) is 9.260×10^{-7} m^{2}s^{-1}.

To study the flow near the model, the meshes size at the free surface was set to be denser, as shown in Figure 3. Even if the amount of mesh differs between meshes near and far away from the model, the total meshes number must be kept in a fine mesh region through the suitable mesh gradient along the computational domain. This technique is useful for utilising the computer's memory to manage the increasing number of elements between the mesh planes at the free surface.

Table 4: Properties of fresh water according to ITTC

Temperature t (°C)	Density ρ (kg/m^3)	Dynamic Viscosity μ (Pa.s)	Kinematic Viscosity v (m^2/s)
23	997.54	9.32 x 10^{-4}	9.3442 x 10^{-7}
24	997.3	9.11 x 10^{-4}	9.1315 x 10^{-7}

The structured grid was employed for the whole computational domain. With the addition of the *snappyHexMesh* utility, three-dimensional meshes containing hexahedra (hex) and split-hexahedra (split-hex) were generated. It is automatically generated from triangulated surface geometries or tri-surfaces in *STL* format. The *snappyHexMesh* script is included with *addLayersControls* and *meshQualityControls*. The *addLayersControls* switches on surface insertion, and *meshQualityControls* is the sub-dictionary used to control the mesh quality around the surface, especially at the complex area and edges on the hull.

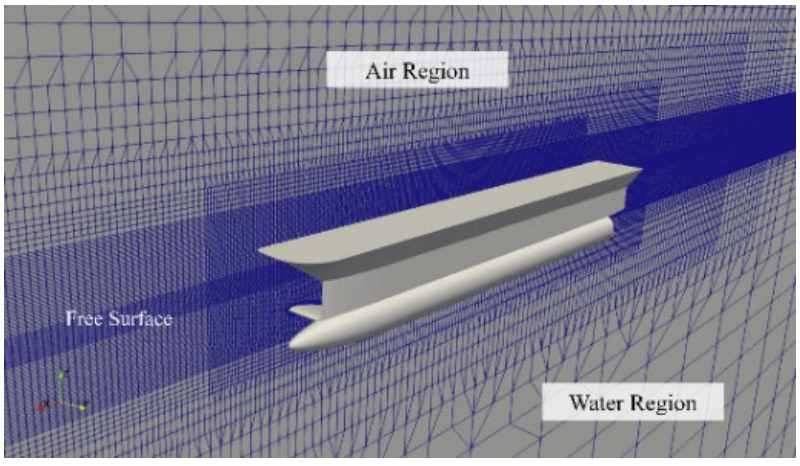

Figure 3: Meshes around the hull.

2.3.2 Boundary and Initial Conditions

Figure 4 shows the boundary conditions defined in the *blockMeshDict* dictionary, which was set up according to the physical properties of the cases. The boundaries were divided into a series of "patches", each of which could be identified by name, as shown in Table 5. The inlet, outlet, atmosphere (top side), and hull were set as patch conditions because they did not contain geometric or topological information about the mesh [22]. These patches were extended to $2L_{OA}$, $4L_{OA}$, and $1.5L_{OA}$ from the model, respectively. Meanwhile, the boundary for the bottom was extended by $3L_{OA}$, and the side was extended by $2L_{OA}$.

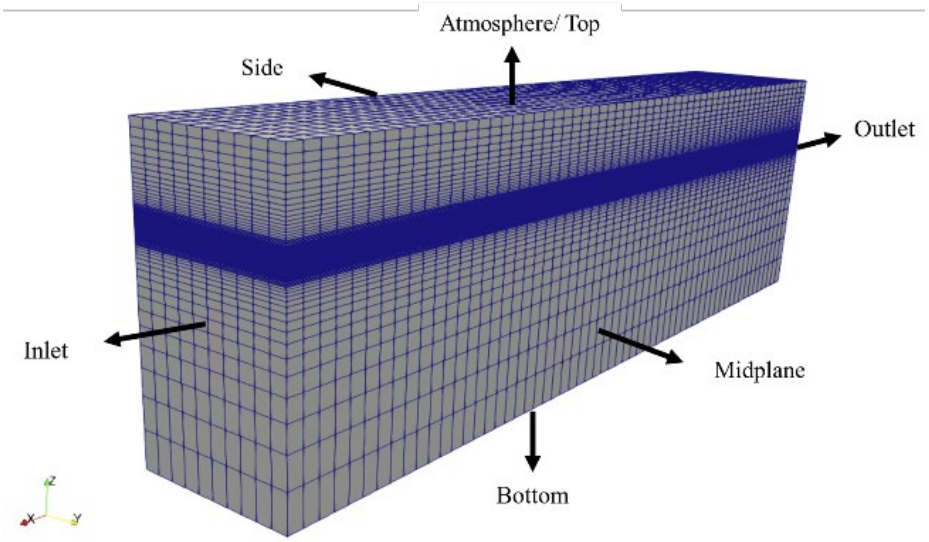

Figure 4 : Boundary conditions in the computational domain.

Table 5 : Boundary conditions for resistance in calm water.

Patch Name	Pressure	Velocity	Turbulence Fields	alpha.water
Inlet	fixedFluxPressure	fixedValue	fixedValue	fixedValue
Outlet	zeroGradient	outletPhaseMeanVelocity	inletOutlet	variableHeightFlowRate
Bottom	symmetry	symmetry	symmetry	symmetry
Midplane	symmetry	symmetry	symmetry	symmetry
Side	symmetry	symmetry	symmetry	symmetry
Atmosphere	totalPressure	pressureInlet OutletVelocity	inletOutlet	inletOutlet
Hull	fixedFluxPressure	movingWall Velocity	omegaWallFunction	zeroGradient

2.3.3 Grid Independent Study

A grid-independent study was conducted to determine the appropriate mesh surrounding the SWATH model. This involved varying the size of the elements near the surface of the SWATH model. Four grid cases, namely G1, G2, G3, and G4 (Table 6) were considered and employed in the model (Figure 5).

Table 6 : Meshing information for the GIS on a hydrofoils-assisted SWATH model at F_r = 0.48.

Meshing case	Number of elements (x 10^6)	R_T (N)	R_F (N)	R_P (N)
G1	0.499	14.405	3.141	11.264
G2	1.100	12.364	3.127	9.237

G3	2.489	11.588	3.113	8.475
G4	4.114	11.496	3.096	8.400

For near-wall treatment, as shown in Figure 5, this study applies y^+ insensitive wall treatment, also known as continuous wall functions. According to [21], this method is valid in the whole boundary layer where the approach of y^+ values is between $1 < y^+ < 300$ and applies to the *k-ω* SST turbulence model. The values of the y^+ for the current study are illustrated in Figure 6, and the values are shown in Table 7, where the values of the y^+ are in an appropriate range. This suggests that the near-wall flow can be accurately resolved.

The outcomes in G3, as shown in Table 7, were consistent with those of G4 (finest mesh) for all resistance components and were used throughout the investigation. While a finer mesh could have theoretically yielded better results, G3 was chosen to manage resource constraints and minimise computation time.

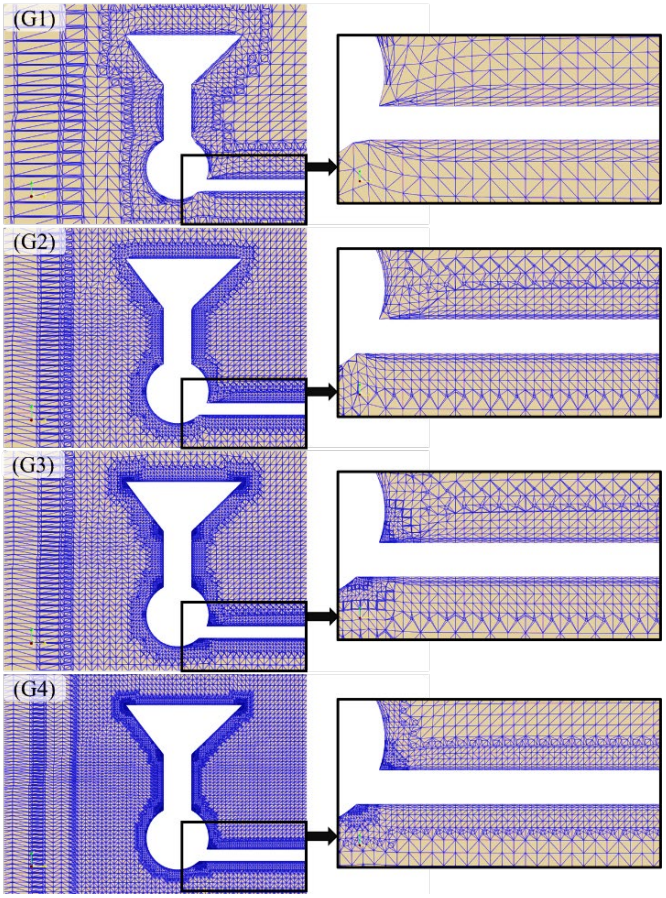

Figure 5 : Different meshes employed on the hydrofoil-assisted SWATH model.

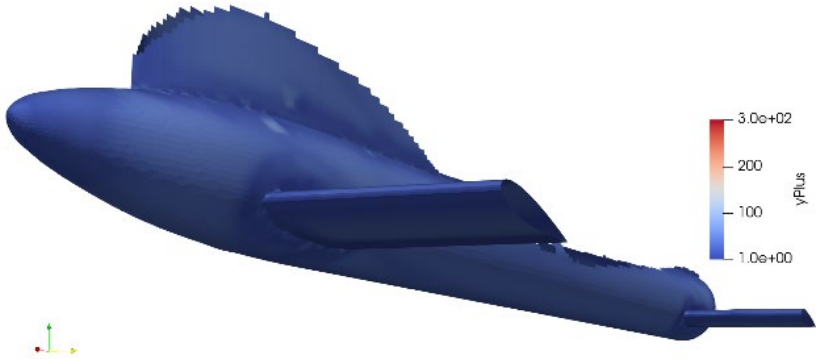

Figure 6 : y^+ distribution on the hull wetted surface

Table 7 : y+ properties for every case.

Mesh Case	y^+ Average Value
G1	43.947
G2	36.904
G3	27.565
G4	16.468

3.0 RESULTS AND DISCUSSION

3.1 Validation for Hydrofoil Assisted SWATH

The experimental and CFD simulation result of total resistance (R_T), friction (R_F), and pressure (R_P) forces are plotted in Figure 7. The relative error between these two approaches reaches up to 7% for the total resistance. Although hull–hydrofoil interaction effects were present, the validation confirmed that the numerical simulation technique can be further developed and applied to the bare hull and demi-hull to estimate the interference factor for the hydrofoil-assisted multihull as conducted in Firdhaus et al. [23] and Chun [24].

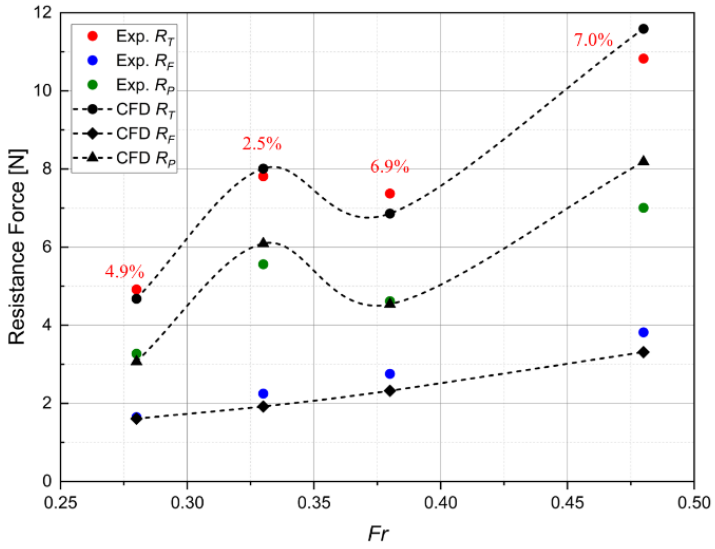

Figure 7 : Comparison between the experimental and numerical simulation results for the hydrofoil assisted SWATH model.

The humps in the resistance curve appear at Froude number 0.33, consistent with previous reports by Chun [22]. This hump appears due to the wave-making interaction when the model moves through the water as the speed increases as shown in Figure 8.

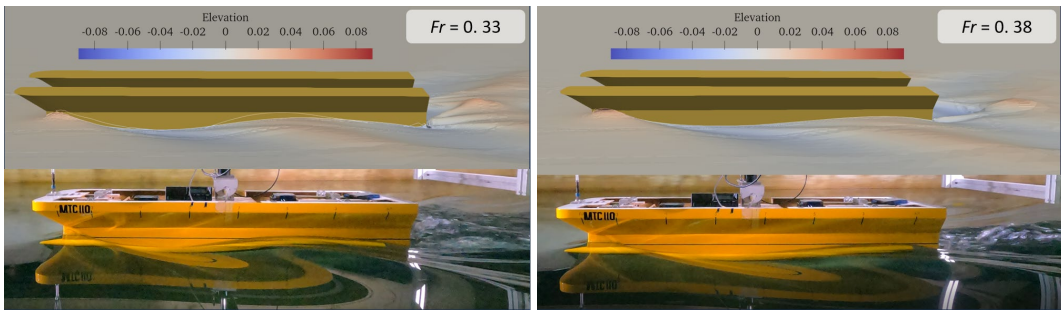

Figure 8: Side-view comparison of the model illustrating the dominance of wave making- resistance at Fr = 0.33 and 0.38

3.2 Hydrodynamics Behavior of SWATH With and Without Hydrofoils

3.2.1 Resistance Comparison

Figure 9 shows the resistance components comprising the total friction and pressure resistance coefficient curves of the SWATH model with and without hydrofoils as a function of Froude numbers. In general, the obtained curve patterns were the same for pressure resistance components. The resistance curve was accompanied by a hump at the initial Froude number (0.28 to 0.33). This hump indicates the wave interference caused by the increased pressure at Froude number 0.33.

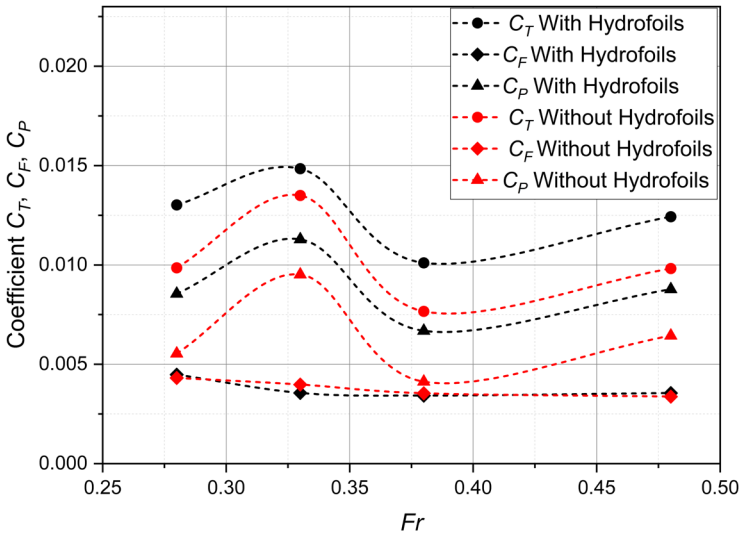

Figure 9 : Coefficient of resistance components for a SWATH model with and without hydrofoils.

As the Froude number increased, the reduction in the frictional resistance coefficient was offset by the increase in pressure resistance coefficient due to a change in speed; Froude number 0.28 to 0.33. As the speed of the model increased, the wave pattern changed, as did the relative positions of crests and troughs. In this process, there was a sequence of speeds at which the crests of the two systems reinforced one another, separated by other speeds at

which crests and troughs tended to cancel one another [22]. It is advantageous to ensure, whenever possible, that the ship operates under service conditions at a favourable speed.

In addition, introducing the hydrofoils increased the total resistance coefficient by 27%, 10%, 27%, and 23% at Froude numbers 0.28, 0.33, 0.38, and 0.48, respectively. The increase in resistance was primarily attributed to the pressure resistance coefficient. As shown in Figure 10, the pressure distribution on the free surface is more pronounced compared to that of the model without hydrofoils. This occurs because, in the hydrofoil-assisted SWATH, additional pressure is generated and dissipated as the hydrofoils interact with the water surface. For brevity, only the pressure distribution at a representative Froude number; Fr = 0.28 and Fr = 0.38 is presented, as it results in highest number of resistance increment percentage.

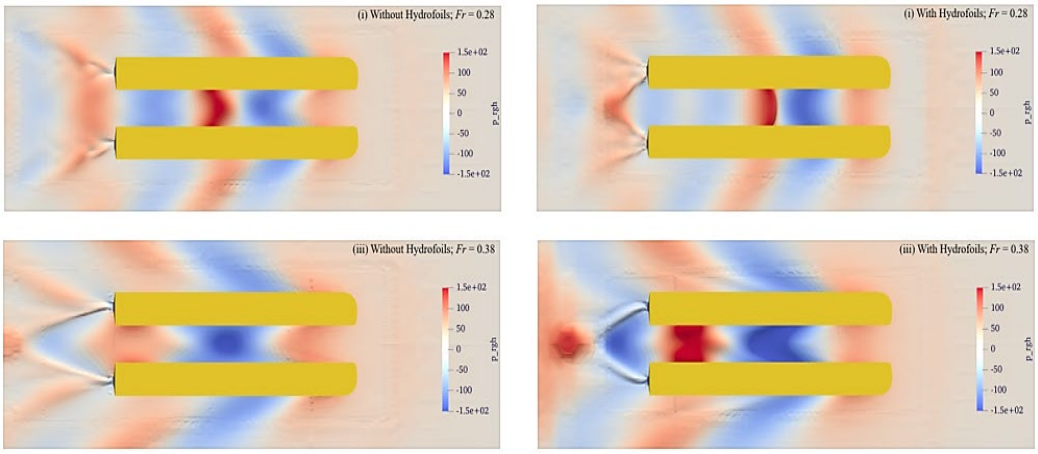

Figure 10: Pressure distribution on the free surface (left) without hydrofoils and with hydrofoils (right).

3.2.2 Motion Comparison

The recorded time responses are shown in Figure 11, illustrating the constant model motion during the test. This event indicated that the effect of the lift generated by the hydrofoils became apparent, as can be seen in Figure 12. The heaves, which indicate the lifting height of the hydrofoil-assisted SWATH when the ship was sailing in calm water, were greater than those without hydrofoils. This is due to the lift force generated by the hydrofoils' rise up the SWATH model from its initial draft. The pitch motion attained by the model without hydrofoils is in a negative area, indicating the reason for the decreasing heave. This phenomenon demonstrates that the model experienced an undesirable condition called the bow-dive effect which is associated with negative pitch values.

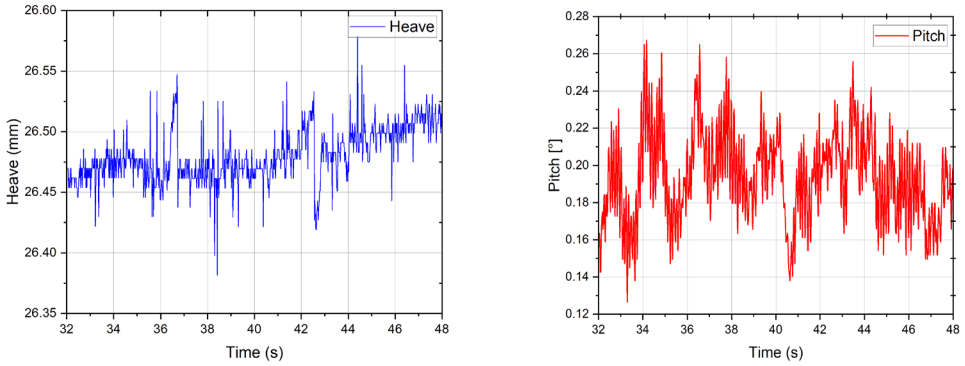

Figure 11: Time-history responses of heave and pitch at Fr = 0.48 with hydrofoils

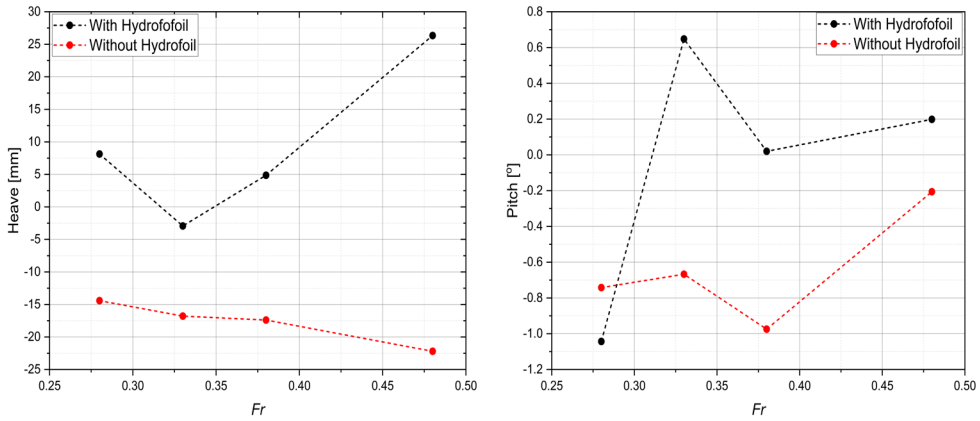

Figure 12: Heave (left) and pitch (right) comparison of the SWATH model with and without hydrofoil.

3.3 Interference Effects

The addition of hydrofoils to the SWATH design system highlighted the importance of considering the interference effect. This was due to the fact that the interference effect affected the hydrodynamic performance as well as the overall efficiency of the system. Comparing the resistance coefficient or resistance force components attained by the hydrofoil-assisted SWATH to those attained by the non-interference hydrofoils-assisted SWATH, which was computed independently, is a method that can be used to ascertain the interference caused by the hydrofoil on the SWATH design. This method allows for the estimation of the impact that this interference had.

To determine the interference effect of the bare hull, a similar approach can be used by comparing these results to those obtained with the demi-hull (monohull case). To enable direct comparison with the catamaran configuration, the resistance of the demi-hull was multiplied by two. It is important to maintain fixed positions for both the demi-hull and the bare hull under similar dynamic conditions (heave and pitch) of the hydrofoils-assisted SWATH. This is being done to guarantee that there are no additional dynamic effects that can have an effect on the data. As a result, a clear distinction between the interference experienced with and without the hydrofoil can be fairly drawn.

The simulation on the demi-hull and bare hull was performed accordingly. To confirm the existence of the interference effect, the resistance coefficient components are plotted in Figure 13 and Figure 14. Figure 13 shows the resistance coefficient components of the hydrofoils-assisted SWATH, with interference and non-interference. Meanwhile, the

comparison of the coefficient resistance components of the bare hull and demi-hull is depicted in Figure 14. From these figures, it can be seen that the major contribution of the difference in total resistance coefficient is the pressure resistance coefficient, C_P. The pattern of the resistance coefficient curves for both hydrofoil-assisted SWATH and bare hull is alike. At the low Froude numbers 0.28 and 0.33, there is a significant improvement in the pressure resistance total resistance coefficient.

The interference factor of hydrofoils-assisted SWATH, η_{SW+H}, can be derived from Equation (3) used by Souto-Iglesias *et. al* [23], Zaghi *et. al* [24], Ali [20], and Begovic *et. al* [1],

$$\eta = \frac{C_T^{(C)} - 2C_T^{(M)}}{2C_T^{(M)}} = \frac{R_T^{(C)} - 2R_T^{(M)}}{2R_T^{(M)}} \tag{2}$$

where C represents catamaran drag and M represents the monohull drag.

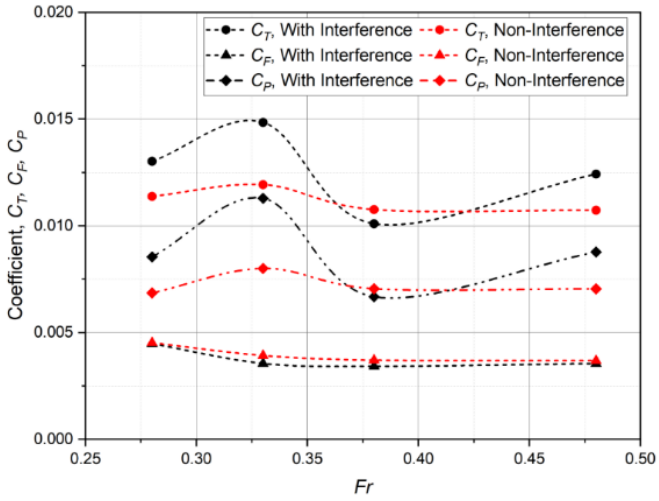

Figure 13: Resistance components of hydrofoils-assisted SWATH with interference (multihull case value) and without interference (the single hull case value multiplied by two).

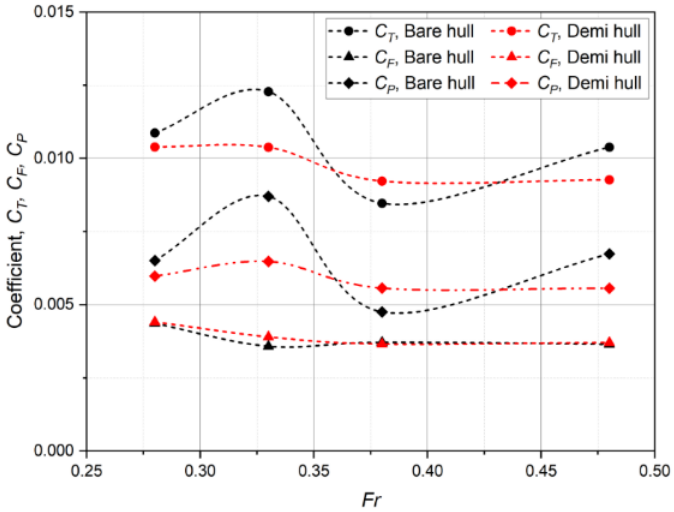

Figure 14 : Resistance components of fixed bare hull and fixed demi-hull.

However, to calculate the interference factor using the resistance coefficient for hydrofoils-assisted SWATH, the running wetted surface, *S*, as in Equation (2), needs to be considered because the value of *S* is different between the hydrofoils-assisted SWATH, demi-hull, and

the hydrofoils. The resistance coefficient of both hydrofoils must also be calculated separately due to different angle of attack, *AoA* (H_1 = 9°; H_2 = 5°). Thus, the modified interference factor of the hydrofoil-assisted SWATH, η_{SW+H}, was addressed as in Equation (4).

$$\eta_{SW+H} = \frac{C_T S^{(SW+H)} - 2C_T S^{(Demi)} - \left(C_T^{(H_1)} + C_T^{(H_2)}\right) S^{(H_1+H_2)}}{2C_T S^{(Demi)} + \left(C_T^{(H_1)} + C_T^{(H_2)}\right) S^{(H_1+H_2)}} = \frac{R_T{}^{(SW+H)} - 2R_T{}^{(Demi)} - R_T^{(H_1)} - R_T^{(H_2)}}{2R_T{}^{(Demi)} + R_T^{(H_1)} + R_T^{(H_2)}} \quad (3)$$

The interference factor for SWATH only or bare hull, η_{SW}, can be defined as Equation (5).

$$\eta_{SW} = \frac{C_T S^{(Bare)} - 2C_T S^{(Demi)}}{2C_T S^{(Demi)}} = \frac{R_T{}^{(Bare)} - 2R_T{}^{(Demi)}}{2R_T{}^{(Demi)}} \quad (4)$$

As shown in Figure 15, the value zero on the *y*-axis indicates zero interference, representing the demi-hull and non-interference SWATH with hydrofoils. From the plotted interference factor curves, the hydrofoil-assisted SWATH encountered greater interference at a wide range of speeds than the one attained by the bare hull. This increment was about 103%, 28%, 29%, and 26% at Froude numbers 0.28, 0.33, 0.38, and 0.48, respectively. The great increment of the interference factor at Froude number 0.28 is because the model experienced a bow-dive effect.

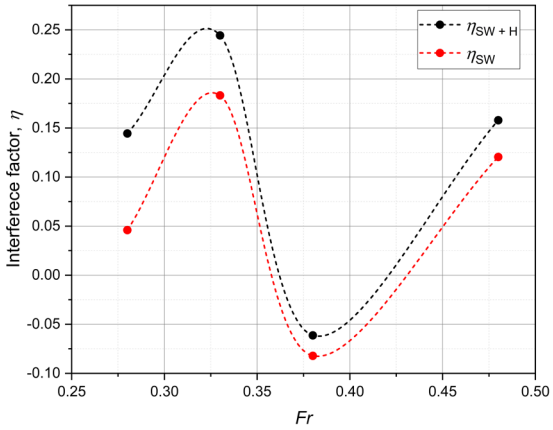

Figure 15: Interference factor of hydrofoils-assisted SWATH and bare hull.

At low Froude numbers (0.28–0.38), a positive interference pattern was observed, forming a pronounced hump that indicates constructive wave interference. The phenomena incline with result of wave interference explained in Zaghi *et. al* [24]. In this region, the bow and stern wave systems of the demi-hulls were in phase, causing the wave crests from each hull to reinforce one another and increase the total wave amplitude. This phenomenon corresponds to a rise in the pressure component of the total resistance coefficient, where the energy associated with the surface wave system becomes dominant. The increase in wave amplitude is also linked to the relatively longer wavelengths generated at these lower speeds, which tend to overlap constructively within the limited hull spacing of the SWATH configuration. The result is a noticeable rise in total resistance, as shown in Figure 13 and Figure 14, consistent with the behavior reported by Lee and Nam [25] and Souto-Iglesias *et. al* [23].

As the Froude number increased toward 0.38, the crest and trough systems from each demi-hull began to fall out of phase, resulting in partial cancellation and a local minimum or "hollow" in the resistance curve. This negative interference represents a condition in which destructive wave interactions reduce the overall wave energy and, consequently, the pressure resistance component. A similar trend for high-speed interference phenomena was also discussed by Kim *et. al* [26]. Beyond this point, at higher Froude numbers (approximately Fr = 0.48), the wave systems realign, producing a new zone of constructive interference. Such periodic transitions between constructive and destructive interference are characteristic of multihull configurations, where the spacing ratio and hull geometry govern the interference wavelength. Understanding this interference pattern is crucial for identifying favourable operating speeds that minimize total resistance while maintaining hydrodynamic efficiency in hydrofoil-assisted SWATH designs.

4.0 CONCLUSION

Overall, the resistance curves estimated by the OpenFOAM show good agreement to the model test. The errors of total resistance predicted by OpenFOAM to the model test are up to 7% which can be considered as acceptable. This indicates that the CFD method is also applicable to the motion response prediction of hydrofoils-assisted SWATH. Normally, the practical accuracy of the simulation is <10% when compared model test such as the study carried out by [27] where the errors is up to 10%.

This study introduced a modified equation (in resistance coefficient) that considers the running wetted surface area for every part of the hydrofoil-assisted SWATH in order to calculate the interference factor. This is due to different wetted surface area, where the previous equation is not suitable for current model in this study.

As expected, the hydrofoil-assisted SWATH had a slightly higher interference factor than the SWATH without hydrofoils, mostly due to the addition of new components (hydrofoils) to the model system. Nevertheless, the hydrofoils-assisted SWATH experienced a significant improvement in both pitch and heave motions. Thanks to the lift force generated from the hydrofoils. These motions help the model to avoid bow dive effect which can cause serious damage to the model.

Numerical simulations were used to analyse the wave field around the hydrofoils-assisted SWATH vessel. The analysis established that the wave field is related to resistance and interference. A zone of possibly beneficial interference was observed at a Froude number of 0.38. At a Froude number of 0.33, the interference reached its maximum possible value. Additionally, the peaks in the C_T curve appeared when the trough was located near the stern.

Future works will include higher Froude numbers, different angles of attack, and various submergence ratios to explore the impact of hydrofoils on SWATH comprehensively. Furthermore, a large experimental campaign is planned to measure wave cuts in both the outer and inner regions for several demi-hull separations and seakeeping tests in both regular and irregular waves.

ACKNOWLEDGEMENT

This research is fully supported by FRGS grant 5F239. The authors fully acknowledged the Ministry of Higher Education (MOHE) for the approved fund and Marine Technology Center for the computing facilities, which makes this important research viable and effective.

REFERENCES

[1] Begovic, E., Bertorello, C., Bove, A., & De Luca, F., Experimental study on hydrodynamic performance of SWATH vessels in calm water and in head waves. *Applied Ocean Research*, 2019. **85**: p. 88-106.DOI:https://doi.org/10.1016/j.apor.2018.10.012
[2] Qian, P., Yi, H., & Li, Y., Numerical and experimental studies on hydrodynamic performance of a small-waterplane-area-twin-hull (SWATH) vehicle with inclined struts. *Ocean Engineering*, 2015. **96**: p. 181-191.DOI:https://doi.org/10.1016/j.oceaneng.2014.12.039
[3] Wang, J., Zhuang, J., & Su, Y., A study on longitudinal motion stability of a variable-structure SWATH USV with and without twin hydrofoils. *Ocean Engineering*, 2022. **265**: p. 112606.DOI:https://doi.org/10.1016/j.oceaneng.2022.112606
[4] Wang, H.D., Qian, P., Liang, X.F., & Yi, H., Vertical plane motion control of an S-SWATH vehicle with flapping foil stabilisers sailing in waves. *Ocean Engineering*, 2016. **121**: p. 184-195.DOI:https://doi.org/10.1016/j.oceaneng.2016.05.004
[5] Sun, X.S., Yao, C.B., Xiong, Y., & Ye, Q., Numerical and experimental study on seakeeping performance of a SWATH vehicle in head waves. *Applied Ocean Research*, 2017. **68**: p. 262-275.DOI:https://doi.org/10.1016/j.apor.2017.09.010
[6] Ali, A., Maimun, A., & Ahmed, Y.M., Analysis of Resistance and Generated Wave around Semi SWATH Hull at Deep and Shallow Water. *Journal of Advanced Research in Fluid Mechanics and Thermal Sciences*, 2019. **58**(2): p. 247-260
[7] Rahimuddin, R., *Seakeeping Performance of Semi-SWATH Ship in Following Sea Using Controlled Fins Stabilizer*, in *Faculty of Mechanical Engineering*. 2013, Universiti Teknologi Malaysia.
[8] Najafi, A., Aliakbari, T., & Hashemi, S.A., Experimental optimization of hydrodynamic performance of catamarans using hydrofoil element. *Proceedings of the Institution of Mechanical Engineers, Part M: Journal of Engineering for the Maritime Environment*, 2019. **233**(2): p. 488-501.DOI:https://doi.org/10.1177/1475090218761415
[9] Bi, X., Shen, H., Zhou, J., & Su, Y., Numerical analysis of the influence of fixed hydrofoil installation position on seakeeping of the planing craft. *Applied Ocean Research*, 2019. **90**: p. 101863.DOI:https://doi.org/10.1016/j.apor.2019.101863
[10] Kazemi Moghadam, H., Shafaghat, R., & A., H., Foil Application to Reduce Resistance of Catamaran under High Speeds and Different Operating Conditions. *International Journal of Engineering*, 2019. **32**(1)
[11] Migeotte, G., & Hoppe, K.G. Developments in Hydrofoil Assistance for Semi-Displacement Catamarans. in *1st International Conference High Performance Marine Vehicles (HIPER*. 1999.
[12] Ni, Z., Dhanak, M., & Su, T.-c., Performance of a hydrofoil operating close to a free surface over a range of angles of attack. *International Journal of Naval Architecture and Ocean Engineering*, 2021. **13**: p. 1-11.DOI:https://doi.org/10.1016/j.ijnaoe.2020.11.002
[13] Putranto, T., & Sulisetyono, A., Lift-drag coefficient and form factor analyses of hydrofoil due to the shape and angle of attack. *International Journal of Applied Engineering Research*, 2017. **12**(21): p. 11152-11156
[14] Smith, T.C., & Thomas, W.L. A Survey of Ship Motion Reduction Devices. 1990.
[15] Suastika, K., Nadapdap, G.E., Aliffrananda, M.H.N., Hermawan, Y.A., Utama, I.K.A.P., & Aryawan, W.D., Resistance Analysis of a Hydrofoil Supported Watercraft (Hysuwac): A Case Study. *CFD Letters*, 2022
[16] Karim, M.M., Prasad, B., & Rahman, N., Numerical simulation of free surface water wave for the flow around NACA 0015 hydrofoil using the volume of fluid (VOF) method. *Ocean Engineering*, 2014. **78**: p. 89-94.DOI:https://doi.org/10.1016/j.oceaneng.2013.12.013
[17] Prasad, B., Hino, T., & Suzuki, K., Numerical simulation of free surface flows around shallowly submerged hydrofoil by OpenFOAM. *Ocean Engineering*, 2015. **102**: p. 87-94.DOI:https://doi.org/10.1016/j.oceaneng.2015.04.049
[18] Uddin, M.I., & Karim, M.M., Application of Volume of Fluid (VOF) Method for Prediction of Wave Generated by Flow around Cambered Hydrofoil. *Procedia Engineering*, 2017. **194**: p. 82-89.DOI:https://doi.org/10.1016/j.proeng.2017.08.120
[19] Ochi, K.M., *Hydroelastic study of a ship equipped with an antipitching fin*, in *Annual Meeting, Society of Naval Architects and Marine Engineers*. 1961: New York
[20] Ali, A., *Effects of Fin Stabilizers Configurations on Semi SWATH Resistance*. 2017, Universiti Teknologi Malaysia.
[21] Guerrero, J., OpenFOAM advanced training. *Turbulence Modeling in General CFD and OpenFOAM—Theory and Applications*, 2022
[22] Chun, H.-H., A comparison of hydrodynamic characteristics of single and tandem strut SWATH ships. *Journal of the Society of Naval Architects of Korea*, 1992. **29**(3): p. 102-116
[23] Souto-Iglesias, A., Zamora-Rodríguez, R., Fernández-Gutiérrez, D., & Pérez-Rojas, L., Analysis of the wave system of a catamaran for CFD validation. *Experiments in Fluids*, 2007. **42**(2): p. 321-332.DOI:https://doi.org/10.1007/s00348-006-0244-4

[24] Zaghi, S., Broglia, R., & Di Mascio, A., Analysis of the interference effects for high-speed catamarans by model tests and numerical simulations. *Ocean Engineering*, 2011. **38**(17): p. 2110-2122.DOI:https://doi.org/10.1016/j.oceaneng.2011.09.037

[25] Lee, W., & Nam, B.W., Numerical Analysis of Wave Interference Effects on Ship Resistance in Parallel Arrangements. *J. Ocean Eng. Technol.*, 2024. **38**(6): p. 325-335.DOI:https://doi.org/10.26748/KSOE.2024.082

[26] Kim, D.J., Kim, S.Y., You, Y.J., Rhee, K.P., Kim, S.H., & Kim, Y.G., Design of high-speed planing hulls for the improvement of resistance and seakeeping performance. *International Journal of Naval Architecture and Ocean Engineering*, 2013. **5**(1): p. 161-177.DOI:https://doi.org/10.2478/IJNAOE-2013-0124

[27] Lotfi, P., Ashrafizaadeh, M., & Kowsari Esfahan, R., Numerical investigation of a stepped planing hull in calm water. *Ocean Engineering*, 2015. **94**: p. 103-110.DOI:https://doi.org/10.1016/j.oceaneng.2014.11.022